BIOCHEMISTRY
including biophysical chemistry & molecular biology

Article

pubs.acs.org/biochemistry

Multimerization of Solution-State Proteins by Tetrakis(4-sulfonatophenyl)porphyrin

Oleksandr Kokhan,[†] Nina Ponomarenko,[†,§] P. Raj Pokkuluri,[‡] Marianne Schiffer,[‡] and David M. Tiede*[,†]

[†]Chemical Sciences and Engineering Division, Argonne National Laboratory, Lemont, Illinois 60439, United States

[‡]Biosciences Division, Argonne National Laboratory, Lemont, Illinois 60439, United States

Supporting Information

ABSTRACT: Surface binding and interactions of anionic porphyins bound to cationic proteins have been studied for nearly three decades and are relevant as models for protein surface molecular recognition and photoinitiated electron transfer. However, interpretation of data in nearly all reports explicitly or implicitly assumed interaction of porphyrin with monodisperse proteins in solutions. In this report, using small-angle X-ray scattering with solution phase samples, we demonstrate that horse heart cytochrome (cyt) *c*, triheme cytochrome c_7 PpcA from *Geobacter sulfurreducens*, and hen egg lysozyme multimerize in the presence of zinc tetrakis(4-sulfonatophenyl)porphyrin (ZnTPPS). Multimerization of cyt *c* showed a pH dependence with a stronger apparent binding affinity under alkaline conditions and was weakened in the presence of a high salt concentration. Ferric-cyt *c* formed complexes larger than those formed by ferro-cyt c. Free base TPPS and FeTPPS facilitated formation of complexes larger than those of ZnTPPS. No increase in protein aggregation state for cationic proteins was observed in the presence of cationic porphyrins. All-atom molecular dynamics simulations of cyt *c* and PpcA with free base TPPS corroborated X-ray scattering results and revealed a mechanism by which the tetrasubstituted charged porphyrins serve as bridging ligands nucleating multimerization of the complementarily charged protein. The final aggregation products suggest that multimerization involves a combination of electrostatic and hydrophobic interactions. The results demonstrate an overlooked complexity in the design of multifunctional ligands for protein surface recognition.

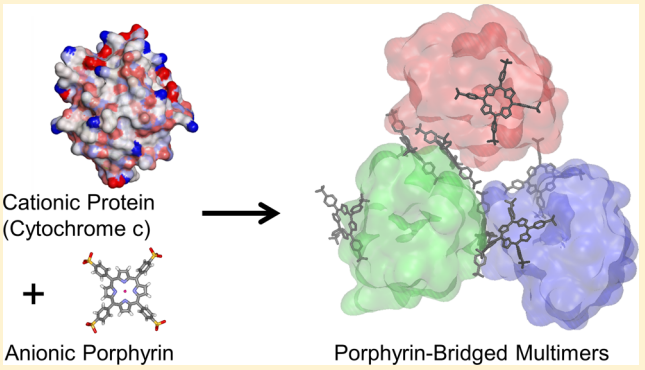

The design of water-soluble, redox-active, molecular complexes for protein surface recognition has been of widespread interest for a range of pharmaceutical, chemical, and biochemical applications.[1−4] Because of their rich optical absorption, emission, and photoinitiating chemical properties, the surface site recognition and docking of water-soluble tetrakis porphyrins and phthalocyanines onto redox cofactor-containing proteins have been extensively studied and continue to serve as useful prototype models for investigating site-specific protein surface recognition and light-initiated electron transfer.

The first studies of docking of porphyrin on a protein surface demonstrated selective hypochromic optical absorption shifts of meso-tetrakis(4-carboxyphenyl)porphyrin upon binding to the positively charged, heme-exposed surface site on cytochrome *c*.[5] Subsequently, a variety of measurements documenting anionic porphyrin fluorescence quenching upon docking to the cytochrome *c* surface corroborated these results and suggested an electron transfer-based quenching mechanism.[6−10] Hamilton and co-workers developed a number of tetrakis porphyrins binding with a high affinity to the surface of cyt *c*[11,12] and argued that such porphyrin−cytochrome complexes demonstrate the possibility of disrupting protein−protein interactions by synthetic surface binding compounds. This work was extended by the demonstration of a significant change in the melting temperature of cytochrome *c*, allowing room-temperature denaturation.[13,14] Solution-state nuclear magnetic resonance (NMR) and modeling studies have mapped the binding of two different porphyrins on the surface of cytochrome *c* and found that a significant part of the protein surface is involved in binding.[15] Analogous but inverse electrostatic assembly has been described for the binding of cationic porphyrins to an anionic plastocyanin docking surface.[16] Goel and co-workers reported X-ray crystal structures of meso-tetrakis(4-sulfonatophenyl)porphyrin (TPPS) with three different carbohydrate-binding proteins.[17−19] The binding sites and mechanisms showed significant variations, but all cases involved hydrogen bond formation between sulfonate groups of TPPS and the target protein, including numerous bridging, interprotein contacts within the crystalline unit cell.[17−19] Purrello et al. demonstrated aggregation of TPPS in the presence of polylysine.[20] Building on this foundation, recent

Received: March 7, 2014
Revised: July 15, 2014
Published: July 16, 2014

dx.doi.org/10.1021/bi500278g | *Biochemistry* 2014, 53, 5070−5079

work has extended protein surface recognition using a range of supramolecular building blocks, including a hemicacerene host, redox−guest complexes,[21] calix[*n*]arenes,[22,23] cucurbit[*n*]urils,[24,25] and cyclodextrins.[26]

However, particularly for the docking of porphyrin to proteins in solution, data analysis and interpretation have relied on an assumption that a single protein molecule interacts with one or more bound supramolecular ligands. To the best of our knowledge, there is only one published report demonstrating synergetic involvement of more than one protein molecule with porphyrins, the stabilization of porphyrin J-aggregates at the interface within a myoglobin dimer assembly in solution.[27]

Small-angle X-ray scattering (SAXS), potentially in combination with NMR measurements, provides a direct, diagnostic technique for the determination of the protein size, radius of gyration, and aggregation state (e.g., reviewed in refs 28−32). A small fraction of the impinging X-ray beam is scattered coherently on sample atoms. This scattering produces an interference pattern that can be recorded with a two-dimensional X-ray detector. Collected scattering data are typically averaged and binned according to the momentum transfer vector $q = (4\pi/\lambda) \sin \theta$, where λ is the X-ray wavelength and θ is half of the scattering angle. In the small-angle region, the scattering patterns asymptotically approach the limiting small-angle intensity $I(0)$ according to the Guinier relationship, where R_g is the radius of gyration corresponding to the mean electron density-weighted atomic distance from the center of mass.[31,33,34] Measurement of $I(0)$ for a molecule can be used to determine the molecular weight or aggregation state of a protein at a known concentration.[28−32,35,36] Further, wide-angle X-ray scattering has been demonstrated to provide a measure of protein secondary and tertiary structures, contributing a scattering pattern "fingerprint" that is characteristic of individual protein folding motifs.[31,32,35−38] Relevant to the study presented here, it was successfully applied in the past to assess partial protein folding for incompletely assembled multiheme *c*-type cytochromes[37] and follow changes as small as those induced by a change in heme oxidation state in cytochrome *c*.[39]

In this report, we explore the interaction of TPPS (**1**), T(MeA)P (**2**), and T(MePy)P (**3**) with three cationic proteins (horse heart cytochrome *c*, PpcA, a three-heme cytochrome c_7 from *Geobacter sulfurreducens*, and hen egg lysozyme) using small-angle X-ray scattering. Heme-based fluorescence quenching has been investigated extensively with single-cofactor cytochromes *c*,[6−10] particularly in the context of possible excited-state electron transfer. The multiheme PpcA provides an interesting extension to one that includes possibilities for initiating rapid interheme electron transfer. With all three proteins, we have observed that addition of a stoichiometric amount of porphyrin induces unexpected protein multimerization. Characteristic differences are seen in the multimers formed in each case. Compared to cyt *c* and lysozyme, PpcA showed the interesting property of restricted multimerization, resulting in the formation of dimers in the presence of anion porphrins that indicates a single interaction surface. Porphyrin fluorescence quenching accompanies cytochrome multimerization. Molecular dynamics simulations that included multiple cytochrome and porphyrin molecules within an explicit solvent molecule-containing box confirm the porphyrin-induced multimerization observed in experiments and suggest a mechanism that involves a combination of electrostatic and hydrophobic interactions. The results demonstrate a complexity in the design of multifunctional ligands for protein surface recognition.

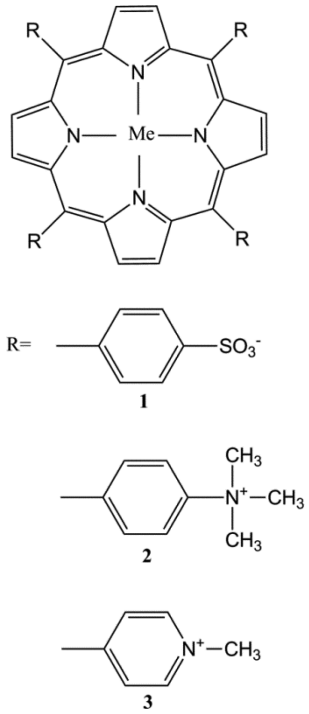

MATERIALS AND METHODS

Recombinant PpcA from *G. sulfurreducens* was produced in the *Escherichia coli* expression system described by Londer et al.[37] with modifications described by Pokkuluri et al.[40] Protein isolation and purification followed the previously published procedure[37] with an additional gel filtration included as a final step. Horse heart cyt *c* and hen egg lysozyme were purchased from Sigma-Aldrich. Zinc, iron, and free base meso-tetra(4-sulfonatophenyl)porphine chloride (ZnTPPS, FeTPPS, and H_2TPPS, respectively), meso-tetra(*N*-methyl-4-pyridyl)-porphine tetratosylate [T(MePy)P], and meso-tetra(4-*N*,*N*,*N*-trimethylanilinium)porphine tetrachloride [T(MeA)P] were purchased from Frontier Scientific (Logan, UT). All other reagents were from Sigma-Aldrich.

X-ray scattering data were acquired with 0.1−1 mM protein samples in 10 mM Tris buffer (pH 7.5) unless indicated otherwise, at the 12-ID-B beamline of the Advanced Photon Source of Argonne National Laboratory (Lemont, IL). To minimize X-ray damage, protein samples were gently refreshed with a syringe pump. A Pilatus 2M detector was used for collecting small-angle X-ray scattering data and provided *q* range coverage from 0.015 to 0.75 Å^{-1}. Wide-angle X-ray scattering data were acquired with a Pilatus 300k detector and had a *q* range of 0.75−2.1 Å^{-1}. Typically, 20 sequential images were collected with a 2 s exposure time per image with each detector. *q* range calibration was performed with a silver behenate sample. The buffer scattering data were subtracted from sample data, and the water peak near $q = 1.9$ Å^{-1} was used as a control in subtractions.

For molecular dynamics simulation, the initial atom coordinates for horse heart cytochrome *c* and PpcA were from Protein Data Bank entries 1AKK and 2LDO. Input files for the simulations were prepared with PSFGEN, SOLVATE, and IONIZE plugins of VMD.[41] The simulations were performed with periodic boundary conditions, and each unit

dx.doi.org/10.1021/bi500278g | *Biochemistry* 2014, 53, 5070−5079

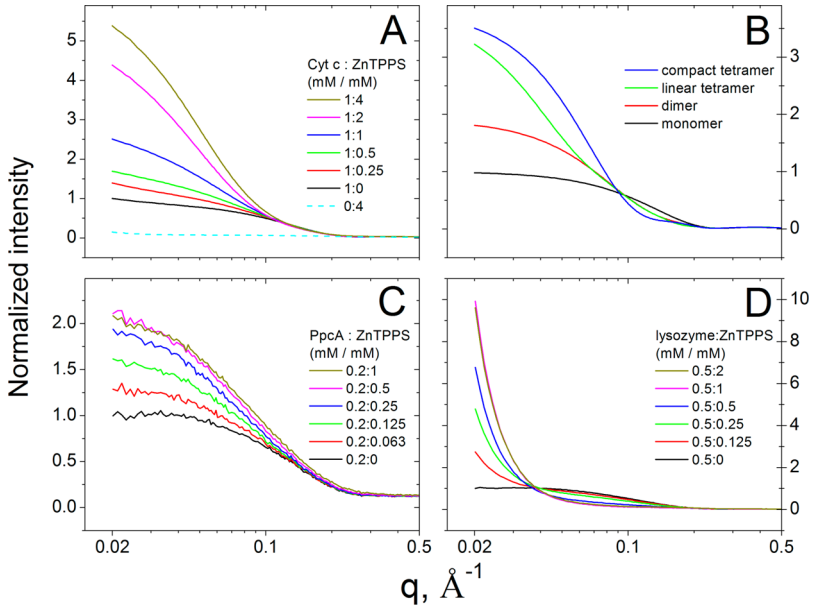

Figure 1. Small-angle X-ray scattering studies of anionic porphyrin-induced multimerization of selected cationic proteins. Panel A shows SAXS profiles for horse heart cytochrome *c* (1 mM) measured in the presence of ZnTPPS with the concentration range of 0−4 mM. Panel B shows calculated scattering profiles for horse heart cytochrome *c* as a monomer and for selected dimer and tetramer models, plotted with the experimental *q* range. PpcA from *G. sulfurreducens* (C) and hen egg lysozyme (D) in the presence of ZnTPPS. Contribution of free ZnTPPS to small-angle scattering of protein samples was negligible (cyan dashed line in panel A).

cell contained four copies of the protein and eight copies of free base TPPS. The unit cell sizes were approximately 52 Å × 101 Å × 116 Å and 56 Å × 94 Å × 116 Å for cyt *c* and PpcA, respectively, and contained ∼55000 atoms. The initial distances between the centers of proteins were at least 45 Å. Sodium and chloride ions were added to make the total ionic strength 100 mM and to neutralize these systems. The simulations were performed with the CHARMM27 force field.[42] Force field parameters for the *c*-type heme of cytochrome *c* were from ref 43. The charge distribution was modified for *c*-type hemes of PpcA to reflect their different axial ligation (His/His). All-atom molecular dynamics simulations were performed with NAMD2[44] on the Fusion cluster of the Laboratory Computing Resource Center at Argonne National Laboratory. MD simulations were run with the following settings: *NPT* (P = 1 atm; T = 310 K), 1 fs integration time, and 12 Å cutoff distance. Nonbonded forces were calculated every two steps, and electrostatic forces were calculated every four steps using the particle mesh Ewald method. Pressure and temperature were maintained with a Langevin piston and bath as implemented in NAMD2. Atom coordinates were recorded each 10 ps. Three independent simulations were run for 140−150 ns for cyt *c* and 90 ns for PpcA. Analysis of MD trajectories was performed with VMD.

RESULTS

Prior studies of binding of anionic porphyrins to cytochrome *c* have relied upon measurement of the quenching of the porphyrin fluorescence for cytochrome *c*. Binding of ZnTPPS to cyt *c* shows fluorescence quenching similar to that of other anionic porphyrins (Figure S1 of the Supporting Information). To verify the binding stoichiometry and to explore the binding of porphyrin to proteins not containing hemes, we studied binding of ZnTPPS to cyt *c*, PpcA, and lysozyme using small-angle X-ray scattering (SAXS) (Figure 1). On the basis of their protein sequences and assuming full protonation of histidine residues and full ionization of aspartate, glutamate, lysine, and arginine residues as well as the heme propionic acid groups, these proteins are expected to have net charges of +8, +4, and +8, respectively. In each case, the addition of ZnTPPS was found to cause significant changes in the small-angle scattering that are indicative of a marked multimerization.

Figure 1A shows solution scattering profiles for cytochrome *c* and ZnTPPS mixtures with the mole ratio varied from 0 to 4. The measurements demonstrate a significant increase in small-angle scattering intensity for cytochrome *c* upon addition of ZnTPPS, even at substoichiometric ratios. The extrapolated magnitude of scattering, $I(0)$, was observed to increase 2.5-fold for 1 mM oxidized cyt *c* upon addition of 1 mM ZnTPPS and to increase 5.4-fold with 4 mM ZnTPPS (Figure 1A). For comparison, Figure 1B shows scattering patterns calculated for a series of monomer, dimer, linear, and compact tetramer models (Figure S2 of the Supporting Information) for cytochrome *c* and plotted with the experimental *q* range. Because $I(0)$ is approximately proportional to the product of the protein concentration and molecular weight squared of the protein complex, multimerization at a fixed cytochrome concentration is reflected by a linear increase in $I(0)$ that scales directly with aggregation number.

The scattering intensity from 4 mM ZnTPPS is negligible in comparison with the scattering intensity from the protein at a small angle. A Guinier plot from these data (Figure S3 of the Supporting Information) yields an apparent R_g of 6.71 Å, which is a good match to the radius of gyration calculated from the atomic coordinates of the HIYBEY structure from the Cambridge Structural Database using SolX.[33,45] This indicates that ZnTPPS is in the monodisperse form in solution over a range of concentrations at least up to 4 mM.

All previous reports of interaction of cyt *c* with porphyrins assumed a 1:1 binding stoichiometry and a monodisperse solution state of cytochrome (see, e.g., refs 7, 9, and 11). The observed significant changes in scattering for cyt *c* upon

dx.doi.org/10.1021/bi500278g | *Biochemistry* 2014, 53, 5070−5079

ZnTPPS addition cannot be explained by binding of one porphyrin per cytochrome in its monodisperse form because binding of ZnTPPS adds ~10% to the molecular weight. Even addition of 250 μM ZnTPPS to 1 mM cyt *c* resulted in an approximately 40% increase in the scattering intensity. The solution-state X-ray scattering data of 4 mM ZnTPPS in the absence of proteins (cyan trace in Figure 1A) show a negligible contribution and suggest that ZnTPPS in the range of concentrations used in our experiments was in its monodisperse form. The observed significant changes in the scattering intensities at low values of momentum transfer together with an increase in gyration radii suggest that addition of ZnTPPS induces cyt *c* multimerization. The limited number of titration points does not allow the binding stoichiometry to be unequivocally established, but it appears that at low porphyrin concentrations, one ZnTPPS molecule can facilitate formation of cyt *c* dimers while with a 4-fold molar excess of porphyrin we observed complexes consisting of five to six cyt *c* monomers. Further, the examination of scattering calculated from model aggregates shows that the degree to which the scattering curve dips below that of the monomer in the *q* range from 0.1 to 0.2 Å^{-1} is related to the fraction of the cytochrome surface occupied in the multimer assembly. For example, this effect is more significant with a compact tetramer that has more of the cytochrome surface involved in protein−protein contact compared to a linear tetramer (Figure 1B). A comparison to the experimental scattering patterns suggests a "looser" association in the experiment than in the models. Further modeling studies will provide more detailed information about the cytochrome *c* multimer structure.

A lesser extent of ZnTPPS-induced multimerization was observed with PpcA, a member of the three-heme cyt c_7 family, from *G. sulfurreducens* (Figure 1C). Similar to the results of the cyt *c* titration, PpcA multimerization was noticeable even with substoichiometric amounts of ZnTPPS. However, unlike cyt *c*, which formed larger multimers with increasing concentrations of ZnTPPS, the titration with PpcA showed saturation. The protein−porphyrin complex sizes are found to be equivalent with both 2.5- and 5-fold excesses of ZnTPPS. The limited, approximately 2-fold increase in $I(0)$ for PpcA induced by the addition of excess ZnTPPS suggests a transition to an aggregation state that consists principally of dimers. Multimerization that self-limits to a dimer would be consistent with an association mechanism driven by a single ligand binding site on the protein surface.

Figure 2 shows that porphyrin core metal and cytochrome concentration have significant impacts on the size of cytochrome *c* multimers. In experiments conducted with 100 μM oxidized cyt *c* (i.e., protein concentration 10-fold lower than what was used to obtain data shown in Figure 1A), we still observed cyt *c* multimerization, although with different binding isotherms. With a 4-fold molar excess of ZnTPPS, we observed the formation of protein complexes with an apparent molecular weight approximately 2 times higher than that of monomeric cyt *c*, in contrast to the 5.4-fold increase seen at higher cytochrome concentration. Interestingly, despite the 2-fold lower net charge of Fe(III)TPPS, a titration with this porphyrin revealed the formation of substantially larger protein multimers. A titration with free base TPPS showed an association isotherm, with a limiting increase in size that is larger than that achieved with ZnTPPS at substoichiometric ratios but more closely resembled the titration with ZnTPPS at higher porphyrin concentrations. Our X-ray scattering data suggest

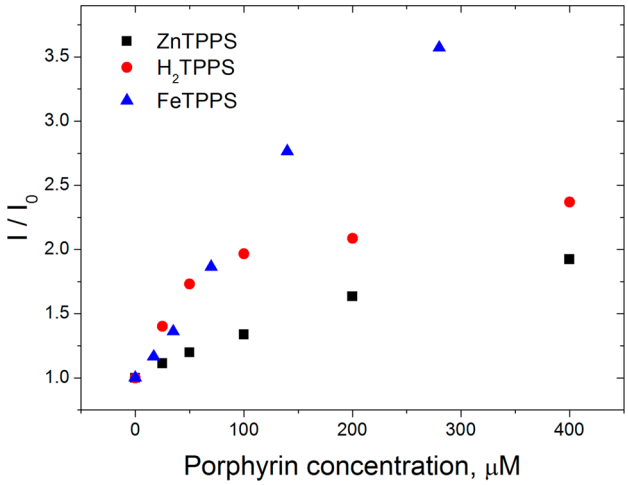

Figure 2. Effect of porphyrin core metal on multimerization of 100 μM horse heart cytochrome *c* as seen from changes in X-ray scattering intensity: black squares for ZnTPPS, blue triangles for Fe(III)TPPS, and red circles for free base TPPS.

that both porphyrin binding and cytochrome multimerization are affected by metal in the core of the porphyrin molecule. The difference in the binding affinity can be best explained by taking into account that zinc in ZnTPPS can form only one axial bond with the protein while the iron of Fe(III)TPPS can form one bond on each side of the porphyrin molecule plane and the core of H_2TPPS can form hydrogen bonds on both sides, as well.

The titration data of the types presented in Figures 1 and 2 provide information about the association constants, K_d, for protein−porphyrin associations. Our preliminary analysis has shown that the extraction of the apparent K_d is complicated by the need to consider contributions from a range of mono- and multimeric protein states as possible minority species. These more detailed quantitative binding studies combined with structural analyses will be reported elsewhere. These data emphasize the distinction in aggregation end states detected for three different cationic proteins in the presence of a 5-fold stoichiometric excess of ZnTPPS. A dimer is found to be formed for PpcA, while a 5−6-multimer aggregate is found for cyt *c*; an extended assembly is found for lysozyme, having dimensions that exceed the low-angle SAXS resolution range used in these experiments.

To evaluate the role of electrostatic forces and their relative contribution to porphyrin-induced cyt *c* multimerization, we compared solution-state small- and wide-angle X-ray scattering of cyt *c* with two cationic porphyrins, T(MeA)P and T(MePy)P, in their free base forms (Figure 3A). Unlike the significant increase in the scattering intensity observed after addition of ZnTPPS (Figure 3A, red line) to oxidized cyt *c* (Figure 3A, black line), mixing cyt *c* with a 2-fold molar excess of either T(MeA)P or T(MePy)P did not produce any statistically significant changes in SAXS and WAXS data (Figure 3A), and the Guinier plots were identical (Figure 3B). This demonstrates that two tested cationic porphyrins do not bind and do not induce multimerization of positively charged cyt *c* under neutral-pH conditions. It also indicates that van der Waals interactions and formation of axial bonds between porphyrin and cytochrome are not sufficient to overcome electrostatic repulsion in such systems.

dx.doi.org/10.1021/bi500278g | *Biochemistry* 2014, 53, 5070−5079

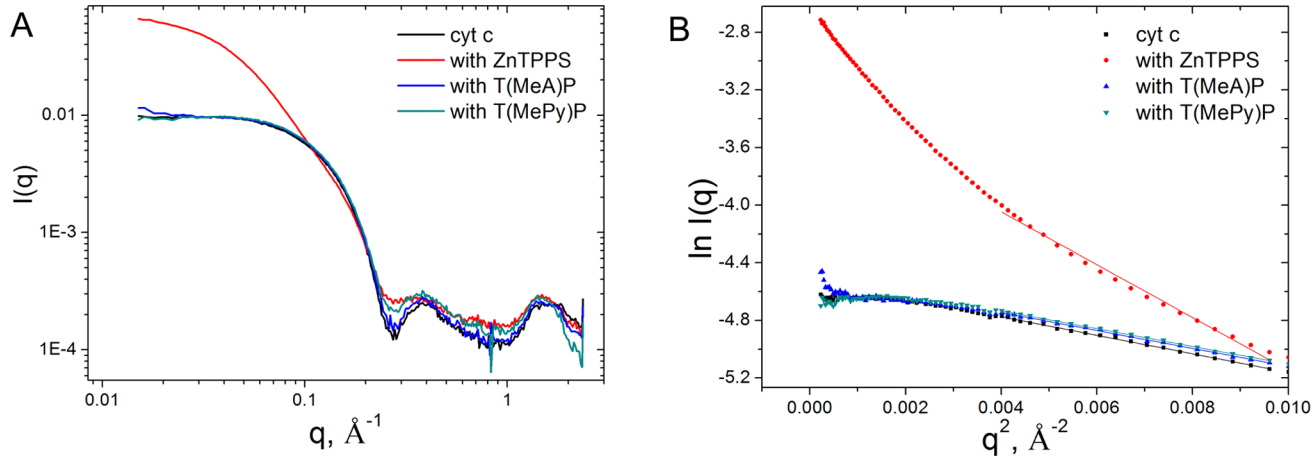

Figure 3. Effect of porphyrin charge on cyt *c* multimerization. (A) Combined small- and wide-angle X-ray scattering profiles for 500 μM cyt *c* without (black) and with 1 mM porphyrins: ZnTPPS (red), free base T(MeA)P (blue), and T(MePy)P (cyan). (B) Guinier plots of cyt *c* with prophryins demonstrate multimerization of cyt *c* in the presence of ZnTPPS and no statistically significant change in the gyration radii in the presence of T(MeA)P or T(MePy)P. The color coding for panel B is the same as that in panel A.

Further, wide-angle X-ray scattering features provide a monitor of characteristic protein secondary and tertiary structural features.[31,32,35−38] The WAXS data for porphyrin−cyt *c* complexes (Figure 3A) show the same features, a trough at q = 0.27 Å and a local maximum at q = 0.39 Å, as the free cyt *c* solution. However, background scattering that appears in the q range above 0.1 Å^{-1} from the remaining porphyrin in solution was not completely removed from these data. The retention of the characteristic WAXS "fingerprint" for cyt *c* indicates that ZnTPPS binding does not significantly perturb the folding or tertiary structure.

To further investigate the role of electrostatic interactions and factors that control multimerization, we explored the pH dependence of the average size of cyt *c* multimers as a function of ZnTPPS concentration (Figure 4). We found a relatively weak pH dependence with the strongest protein complex assembly occurring at pH 8.5. Because ZnTPPS does not have

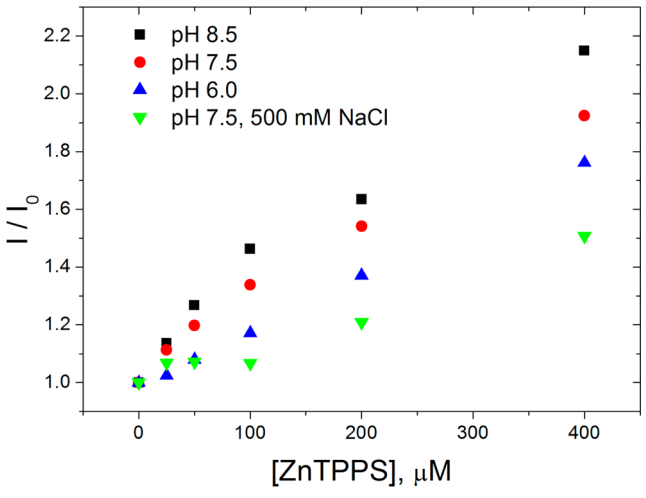

Figure 4. Effect of pH and ionic strength on multimerization of cyt *c* as seen from changes in small-angle X-ray scattering intensity (ratio of Guinier plot intercepts) in titrations of 100 μM oxidized cyt *c* with ZnTPPS in 10 mM Tris buffer (pH 7.5) (red circles), 10 mM Tris buffer (pH 8.5) (black squares), 10 mM MES buffer (pH 6.0) (blue triangles), and 10 mM Tris (pH 7.5) with 500 mM NaCl (green triangles).

protonatable groups with pK_a values within the tested range, pH 6−8.5, the observed dependence must be due to interaction of ZnTPPS with one or more residues of cyt *c* with pK_a near this range. A somewhat surprising result, considering the absence of binding and multimerization with cationic porphyrins, was that a significant increase in ionic strength (μ) from ∼10 to 500 mM was not sufficient to prevent cyt *c* multimerization (Figure 4, green triangles). This indicates that while electrostatic interactions make a major contribution to the formation of complexes of cyt *c* with proteins, van der Waals interactions and axial ligation to porphyrins also contribute to multimerization.

The vast majority of previously published research on the interaction of porphyrin with cyt *c* was conducted using the oxidized form of the protein. However, the reduced form of cyt *c* has an equally important physiological role, and numerous reports highlight differences in binding affinity for both redox states of cyt *c* to its physiological binding partners (see, e.g., refs 46−48) as well as the structural protein changes, including changes at the binding interfaces associated with a change in cyt *c* oxidation state.[49,50] To partially fill this gap, we explored multimerization of oxidized and reduced cyt *c* with ZnTPPS and found that the oxidized cytochrome formed larger complexes. However, the difference in the average complex size was relatively small, especially with substoichiometric concentrations of ZnTPPS relative to cyt *c* concentration (Figure 5).

To visualize mutlimerization of cytochromes by porphyrins and gain insight into the molecular factors controlling this process, we performed a series of all-atom molecular dynamics simulations with explicit solvent (TIP3 water) and periodic boundary conditions. As a compromise between gathering sufficient statistics with limited computational resources, our systems contained four copies of the protein and eight free base TPPS molecules per unit cell. These corresponded to concentrations of cyt *c* and TPPS of 8 and 16 mM, respectively. Although the cytochrome concentrations in the simulations exceed the concentrations of 0.1−1 mM used in the experiments presented here, the observation of porphyrin-induced multimerization across this concentration range suggests that the conditions selected for MD simulations provide an acceptable compromise between lower concen-

dx.doi.org/10.1021/bi500278g | *Biochemistry* 2014, 53, 5070−5079

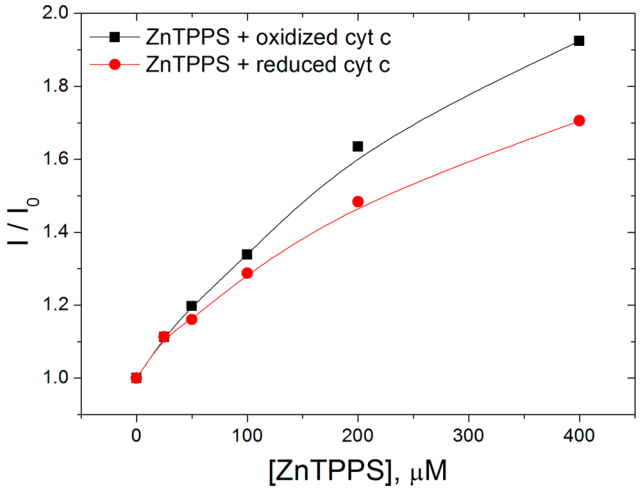

Figure 5. Effect of the heme redox state of cyt *c* on multimerization with ZnTPPS at pH 7.5. Guinier plot intercepts with 100 μM oxidized (black squares) and reduced (red circles) cytochrome *c* as a function of ZnTPPS concentration.

trations used in experiments with higher concentrations needed in simulations sufficient to achieve equilibrium multimerization within computational time scales accessible with current computational resources. Follow-up modeling studies will examine protein and ZnTPPS concentration effects more closely.

For simulations, we used free base TPPS instead of ZnTPPS as classical molecular mechanics simulations can more accurately model formation of hydrogen bonds than protein−transition metal interactions. We performed three independent simulations for both cyt *c* and PpcA. For each protein, we observed TPPS binding to surface sites within a few nanoseconds (Figure 7 and Figures S4 and S5 of the Supporting Information). This process was rapidly followed by the formation of multimers. In the case of PpcA, proteins typically formed either two dimers or linear tetramers (Figure 6B). In contrast, in simulations with cyt *c*, we observed more compact trimers (Figure 6A) and tetramers. Another distinction between these two systems was that typically more porphyrin molecules were bound to the cyt *c* surface and tended to form larger contacts (compare panels A and B of Figure 7). This can be explained by contributions from the smaller total surface area and a larger number of acidic residues per unit area on the PpcA surface imposing more restrictions on possible places for porphyrin binding.

Binding of porphyrins to the surface of cytochrome *c* observed in molecular dynamics simulations was highly dynamic and revealed the involvement of the same protein residues, albeit with somewhat different frequencies in all three independent runs (Figure 7A and Figure S4 and Table S1 of the Supporting Information). The most frequent point of binding of TPPS was observed to be Lys-25 (51.8%) followed by Gly-24, Ala-83, Gly-23, and Lys-86 (43.8, 41.5, 38.2, and 37.6%, respectively). However, a large number of other cytochrome *c* residues were observed within 4 Å of water-soluble porphyrins during the course of all three simulations (see Table S1 of the Supporting Information). The surface area of these residues significantly exceeded the size of TPPS, possibly indicating a number of overlapping binding sites with comparable binding affinities. Interestingly, the residues responsible for binding TPPS formed a contiguous area on

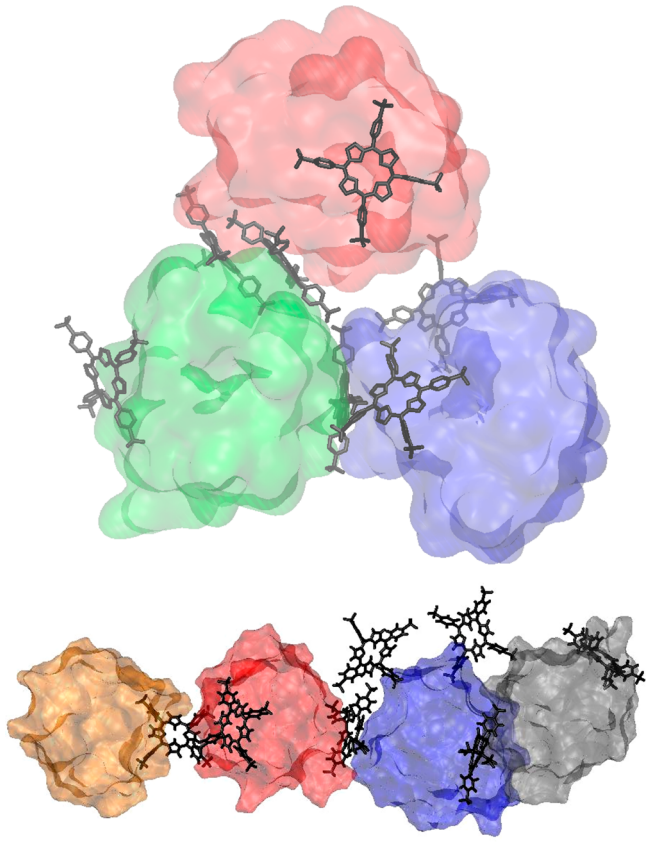

Figure 6. Molecular dynamics simulations performed with four copies of cyt *c* or PpcA per water box demonstrate rapid multimerization. PpcA tended to assemble in dimers or in linear structures (bottom), while cyt *c* formed more globular structures (top).

one side of the protein that significantly overlapped with a ring of lysine residues previously implicated in the binding of cyt *c* to its physiological partners through a number of chemical lysine modification experiments[51−54] as well as the part of cyt *c* seen in X-ray and NMR structures interacting with cytochrome *c* peroxidase,[55,56] the bc_1 complex,[50,57,58] and photosynthetic reaction centers.[59,60] In addition to a significant contribution of electrostatic interactions from lysine residues and polar protein backbone atoms of cyt *c*, our molecular dynamic simulations revealed a contribution from nonpolar interactions consistent with observed multimerization in the presence of 500 mM NaCl. The binding interactions on the molecular level were highly dynamic, which is consistent with reports exploring molecular dynamics simulations of binding of cyt *c* to photosynthetic reaction centers[61] and the bc_1 complex.[62] Finally, the binding area significantly exceeding the size of a porphyrin molecule was recently reported by Crowley and co-workers[15] for binding of coproporphyrin to cyt *c* in their NMR experiments.

In contrast, simulations of binding of TPPS to 3-heme PpcA revealed weaker porphyrin interactions (Figure 7, right panel, and Figure S5 and Table S1 of the Supporting Information). The four residues most frequently forming bonds with TPPS, Asn-10 (44.7%), Cys-65 (40.9%), Lys-9 (39.9%), and Lys-71 (36.1%), were all found to be located on a small patch of protein surface near heme IV and the protein's C-terminus. Dantas and co-workers recently reported that the binding site of negatively charged anthraquinone 2,6-disulfonate on the PpcA surface is also located near heme IV.[63] The proposal for a

dx.doi.org/10.1021/bi500278g | *Biochemistry* 2014, 53, 5070−5079

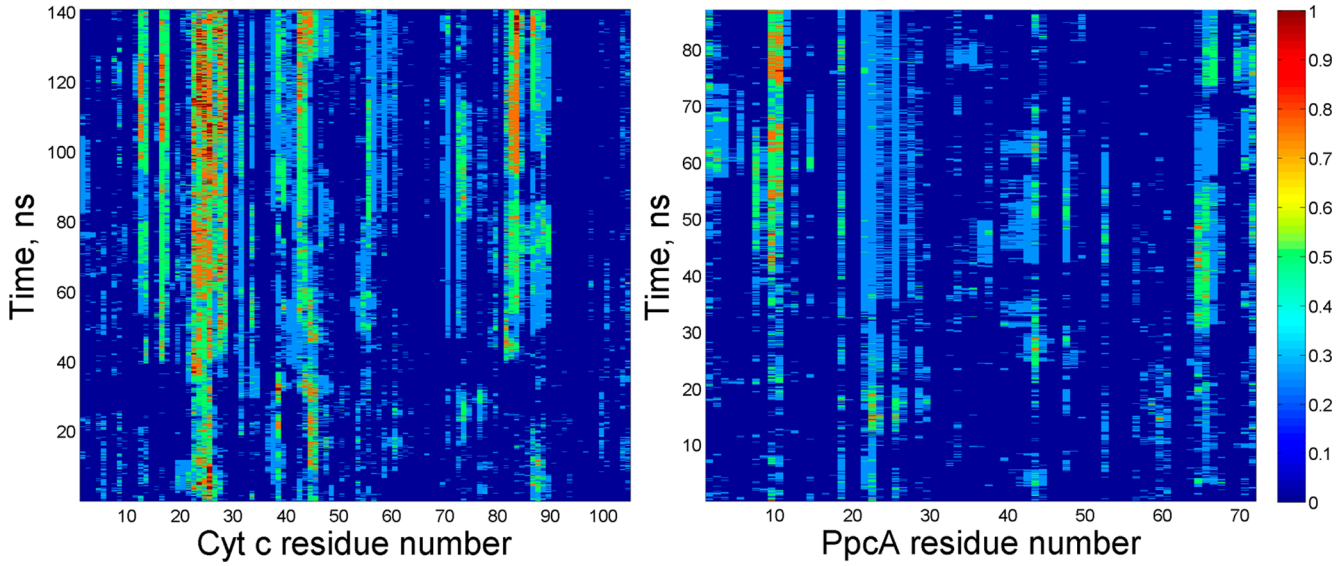

Figure 7. Frequency of binding of free base TPPS to cyt *c* (left) and PpcA (right) in molecular dynamics simulations as a function of time. Horizontal axes give the residue number in respective proteins and vertical axes the time in nanoseconds. Binding of porphyrin to cytochrome is defined here as the presence of at least one non-hydrogen atom of TPPS within 4 Å of a non-hydrogen atom from the protein. Data from the other two simulations for each protein are shown in Figures S4 and S5 of the Supporting Information.

single preferred porphyrin binding site is consistent with the observed dimerization limit for PpcA in our SAXS experiments, while the larger binding area observed in the simulations of cyt *c* can support binding of multiple TPPS molecules and the formation of larger multimers.

DISCUSSION

The design of water-soluble, redox-active, molecular complexes for protein surface recognition have been of widespread interest for a range of pharmaceutical, chemical, and biochemical applications. In this report, we demonstrate that contrary to the commonly assumed 1:1 binding ratio of water-soluble porphyrins to monodisperse protein, a number of cationic proteins formed multimers of variable size in the presence of anionic TPPS. The complex sizes and binding stoichiometries varied for all three tested proteins. In all cases, we observed the formation of dimers when fewer than one porphyrin was present for each two protein molecules. However, with excessive amounts of ZnTPPS with respect to cytochrome *c* or lysozyme, we observed the formation of multimers significantly larger than dimers. In contrast, even with a 4-fold molar excess of ZnTPPS over PpcA concentration, only dimer formation was observed, and a molecular mechanism leading to such a difference in the complex formation pattern will be discussed below.

There are multiple factors that control protein multimerization. From our experiments with cyt *c* and various forms of tetrakis-phenyl porphyrins, we conclude that electrostatic forces play a major role. The high positive surface charge of cyt *c* makes it highly water-soluble. Not surprisingly, negatively charged TPPS can bind to a protein surface with a charge of the opposite sign. However, it bridges positive charges on the protein surface and allows two protein monomers to come to a much closer distance and form a dimer. If protein surfaces are large enough to accommodate binding of multiple porphyrins, this opens the possibility of creating multimers involving more than two proteins. However, our detection of noticeable cyt *c* multimerization with 500 mM NaCl suggests that contributions from forces other than electrostatic are also significant. Similarly, the absence of multimerization with positively charged T(MeA)P and T(MePy)P indicates that van der Waals forces and hydrogen bonding to the nitrogen atoms in the center of the porphyrins are weaker than electrostatics and not sufficient to drive multimerization in the absence of favorable electrostatic attraction or to overcome net electrostatic repulsion with cationic proteins.

The role of axial porphyrin ligation in protein multimerization was demonstrated in experiments with different metals in the core of TPPS. ZnTPPS formed the smallest multimers compared to those of H_2TPPS and Fe(III)TPPS. This observation can be explained by the fact that zinc, in addition to bonds with four nitrogen atoms of the porphyrin, may form an additional metal-coordinated bond with the protein. In contrast, both Fe(III)TPPS and H_2TPPS induced the formation of larger multimers. Unlike pentacoordinated Zn^{2+}, hexacoordinated Fe^{3+} may form bonds with protein on both sides of the porphyrin plane, and the increase in multimer size indicates a significant role of porphyrin axial ligation in the stabilization of multimers. Though free base TPPS is lacking a metal atom in its core, it is capable of forming hydrogen bonds on both sides of its porphyrin plane. Therefore, the formation of larger multimers in the presence of H_2TPPS than with ZnTPPS can be expected.

The observed pH dependence that shows an increased level of multimerization at pH 8.5 compared to that at pH 6 is somewhat surprising. ZnTPPS does not have protonatable groups with pK_a values anywhere near that pH range. Cyt *c* is rich in basic residues, but their pK_a values are too far from the pH 6−8.5 range tested here. Furthermore, even if the pK_a values of those residues are shifted to more neutral values, that would not explain the observed stronger multimerization under more alkaline conditions as there should be a larger fraction of the protonated Lys and Arg residues at pH 6 than at pH 8.5. However, to form hydrogen bonds with the sulfonate groups of TPPS and therefore increase binding affinity, those residues

dx.doi.org/10.1021/bi500278g | *Biochemistry* 2014, 53, 5070−5079

should be in their protonated forms, and we should observe stronger binding under more acidic conditions, the opposite of what we observed in our experiments. Cyt *c* undergoes conformational changes under more extreme pH conditions, but at pH 6−8.5, it stays in its native folded form.[64] This observation leaves a possibility that surface-exposed His-33 or His-26 residues may serve as axial ligands for zinc in ZnTPPS. For the Zn−N_{His} bond to form, the N_ε atom of histidine should be in its deprotonated form. Thus, stronger binding occurs under alkaline conditions with a higher fraction of deprotonated histidine residues. Alternatively, lysine residues can be considered to serve as candidates for axial ligands. It is well established that under alkaline conditions cytochrome *c* undergoes a conformational change and Lys-73 or Lys-79 displaces the native Met-80 ligand of the heme.[64] A similar effect was demonstrated for other *c*-type cytochromes with pK_a values for the alkaline transition as low as 7.9 in the case of *Rhodobacter sphaeroides* cyt c_2.[65] In the absence of competition with a native methionine residue forming a bond with a porphyrin metal atom, it seems reasonable that lysine deprotonation with subsequent binding to the zinc atom of ZnTPPS may occur at the pH range tested in our experiments and can be responsible for the observed pH dependence.

We observed the formation of larger multimers with oxidized cyt *c* compared to the reduced form of the protein. This effect can be due to the overall increase in total protein charge from +7 for ferrous cyt *c* to +8 for ferric cyt *c* under neutral conditions, making binding on ZnTPPS with a −2 charge more energetically favorable. However, the extra charge in the oxidized form of the protein is localized in the vicinity of the heme iron atom, which is buried inside the protein and should have a much smaller contribution than the charges localized on the protein surface. It is feasible that subtle structural changes and differences in surface hydration patterns associated with both redox forms of cyt *c* may play a role in the preferential multimerization of one redox form of the protein akin to stronger binding of ferric cyt *c* to the bc_1 complex[50] and ferrous cyt *c* to photosynthetic reaction centers.[61]

The results of molecular dynamics simulations match our experimental observations based on X-ray scattering and provide additional insight into the molecular mechanism of TPPS-induced protein multimerization. The MD simulations revealed the involvement of electrostatic and hydrophobic interactions in the multimerization of cyt *c* and PpcA. However, cytochrome *c* had a larger porphyrin binding area sufficient to accommodate more than one TPPS molecule bound. Crowley and co-workers[15] reported a similar result based on the NMR shift values observed for binding of coproporphyrin to yeast cytochrome *c*. In this work, they observed significant changes in residues covering nearly half of the protein surface area and spanning more than 20 Å. The authors explained their result as an ensemble of protein−porphyrin interactions with similar binding affinities. While the structural differences of coproporphyrin and ZnTPPS and amino acid sequence variations between yeast and horse heart cytochromes *c* make direct comparison difficult, both studies point to a common mechanism for anionic porphyrin binding involving a combination of electrostatic and hydrophobic interactions with residues covering an area significantly larger than the size of porphyrin molecules in both cases. Further, our work here demonstrates the additional complexity that anionic porphyrins are unexpectedly efficient in supporting bridged, interprotein contacts.

Finally, the differences in the extents of porphyrin-induced multimerization with cyt *c*, PpcA, and lysozyme demonstrate a remarkable control over the multimerization process by the variation in protein surface chemistry. In particular, the discrete dimerization of PpcA suggests the existence of a single site for tetra-sulfonated porphyrin recognition that functions as a bridging ligand between two PpcA molecules. This result corroborates the finding of a single binding site adjacent to heme IV detected by NMR for the humic acid substrate analogue, anthraquinone 2,6-disulfonate (AQDS), which was proposed to be the physiological point for the entry of the electron into PpcA.[63] We conducted X-ray scattering measurements with PpcA in the presence of AQDS and found no shift from the monodisperse state (Figure S6 of the Supporting Information), suggesting that a tetra-sulfonated ligand motif is required to template a ligand-bridged dimer assembly. These considerations suggest opportunities to design redox and photochemically active surface binding ligands for selected protein site recognition and ligand-directed supercomplex assembly. These strategies may provide a means to achieve controlled, ligand-directed electron transfer pathways in PpcA and multiheme architectures. More generally, such directed molecular recognition is relevant for tuning protein interactions for a broad range of pharmaceutical, chemical, and biochemical applications.

■ ASSOCIATED CONTENT

Supporting Information

Supplementary Figures 1−6 and Table 1. This material is available free of charge via the Internet at http://pubs.acs.org.

■ AUTHOR INFORMATION

Corresponding Author

*E-mail: tiede@anl.gov. Phone: (630) 252-3539.

Funding

This work is supported by the Division of Chemical Sciences, Geosciences, and Biosciences, Office of Basic Energy Sciences of the U.S. Department of Energy (DOE), under Contract DE-AC02-06CH11357. Use of the 12-id-B beamline at the Advanced Photon Source, an Office of Science User Facility operated for the DOE Office of Science by Argonne National Laboratory, was supported by the U.S. DOE under Contract DE-AC02-06CH11357.

Notes

The authors declare no competing financial interests.

[§]Consultant contracted by the Argonne National Laboratory from Lab Support, 9450 Bryn Mawr Ave., #340, Rosemont, IL 60018. All work was performed at the Argonne National Laboratory.

■ ACKNOWLEDGMENTS

We gratefully acknowledge the help of Dr. Xiaobing Zuo and the staff of Sector 12 of the Advanced Photon Source at Argonne National Laboratory. In addition, this work benefited from the computing resources provided on "Fusion", a 320-node computing cluster operated by the Laboratory Computing Resource Center at Argonne National Laboratory.

■ ABBREVIATIONS

cyt, cytochrome; SAXS, small-angle X-ray scattering; WAXS, wide-angle X-ray scattering; TPPS, meso-tetra(4-sulfonatophenyl)porphine; T(MePy)P, meso-tetra(*N*-methyl-

4-pyridyl)porphine; T(MeA)P, meso-tetra(4-*N*,*N*,*N*-trimethylanilinium)porphine.

REFERENCES

(1) Lin, Q., Park, H. S., Hamuro, Y., Lee, C. S., and Hamilton, A. D. (1998) Protein Surface Recognition by Synthetic Agents: Design and Structural Requirements of a Family of Artificial Receptors that Bind to Cytochrome c. *Biopolymers 47*, 285−297.

(2) Oshima, T., and Baba, Y. (2012) Recognition of Exterior Protein Surfaces Using Artificial Ligands Based on Calixarenes, Crown Ethers, and Tetraphenylporphyrins. *J. Inclusion Phenom. Macrocyclic Chem. 73*, 17−32.

(3) Shinoda, S., and Tsukube, H. (2011) Molecular Recognition of Cytochrome c by Designed Receptors for Generation of *in vivo* and *in vitro* Functions. *Chem. Sci. 2*, 2301−2305.

(4) Wilson, A. J. (2009) Inhibition of Protein−protein Interactions Using Designed Molecules. *Chem. Soc. Rev. 38*, 3289−3300.

(5) Clark-Ferris, K. K., and Fisher, J. (1985) Topographical Mimicry of the Enzyme Binding Domain of Cytochrome c. *J. Am. Chem. Soc. 107*, 5007−5008.

(6) Cho, K. C., Che, C. M., Ng, K. M., and Choy, C. L. (1986) Electron Transfer between Cytochrome c and Porphyrins. *J. Am. Chem. Soc. 108*, 2814−2818.

(7) Zhou, J. S., Granada, E. S. V., Leontis, N. B., and Rodgers, M. A. J. (1990) Photoinduced Electron Transfer in Self-associated Complexes of Several Uroporphyrins and Cytochrome c. *J. Am. Chem. Soc. 112*, 5074−5080.

(8) Zhou, J. S., and Rodgers, M. A. J. (1991) Driving Force Dependence of Rate Constants of Electron Transfer within Cytochrome c and Uroporphyrin Complexes. *J. Am. Chem. Soc. 113*, 7728−7734.

(9) Larsen, R. W., Omdal, D. H., Jasuja, R., Niu, S. L., and Jameson, D. M. (1997) Conformational Modulation of Electron Transfer within Electrostatic Porphyrin:cytochrome c Complexes. *J. Phys. Chem. B 101*, 8012−8020.

(10) Croney, J. C., Helms, M. K., Jameson, D. M., and Larsen, R. W. (2000) Temperature Dependence of Photoinduced Electron Transfer within Self-assembled Uroporphyrin-cytochrome c Complexes. *J. Phys. Chem. B 104*, 973−977.

(11) Jain, R. K., and Hamilton, A. D. (2000) Protein Surface Recognition by Synthetic Receptors Based on a Tetraphenylporphyrin Scaffold. *Org. Lett. 2*, 1721−1723.

(12) Yin, H., and Hamilton, A. D. (2005) Strategies for Targeting Protein-protein Interactions with Synthetic Agents. *Angew. Chem., Int. Ed. 44*, 4130−4163.

(13) Jain, R. K., and Hamilton, A. D. (2002) Designing Protein Denaturants: Synthetic Agents Induce Cytochrome c Unfolding at Low Concentrations and Stoichiometries. *Angew. Chem., Int. Ed. 41*, 641−643.

(14) Wilson, A. J., Groves, K., Jain, R. K., Park, H. S., and Hamilton, A. D. (2003) Directed Denaturation: Room Temperature and Stoichiometric Unfolding of Cytochrome c by a Metalloporphyrin Dimer. *J. Am. Chem. Soc. 125*, 4420−4421.

(15) Crowley, P. B., Ganji, P., and Ibrahim, H. (2008) Protein Surface Recognition: Structural Characterization of Cytochrome c-Porphyrin Complexes. *ChemBioChem 9*, 1029−1033.

(16) Anula, H. M., Myshkin, E., Guliaev, A., Luman, C., Danilov, E. O., Castellano, F. N., Bullerjahn, G. S., and Rodgers, M. A. (2006) Photo Process on Self-associated Cationic Porphyrins and Plastocyanin Complexes 1. Ligation of Plastocyanin Tyrosine 83 onto Metalloproteins and Electron-transfer Fluorescence Quenching. *J. Phys. Chem. A 110*, 2545−2559.

(17) Goel, M., Jain, D., Kaur, K. J., Kenoth, R., Maiya, B. G., Swamy, M. J., and Salunke, D. M. (2001) Functional Equality in the Absence of Structural Similarity. An Added Dimension to Molecular Mimicry. *J. Biol. Chem. 276*, 39277−39281.

(18) Goel, M., Anuradha, P., Kaur, K. J., Maiya, B. G., Swamy, M. J., and Salunke, D. M. (2004) Porphyrin binding to Jacalin is Facilitated by the Inherent Plasticity of the Carbohydrate-binding Site: Novel Mode of Lectin-ligand Interaction. *Acta Crystallogr. D60*, 281−288.

(19) Goel, M., Damai, R. S., Sethi, D. K., Kaur, K. J., Maiya, B. G., Swamy, M. J., and Salunke, D. M. (2005) Crystal Structures of the PNA-Porphyrin Complex in the Presence and Absence of Lactose: Mapping the Conformational Changes on Lactose Binding, Interacting Surfaces, and Supramolecular Aggregations. *Biochemistry 44*, 5588−5596.

(20) Purrello, R., Bellacchio, E., Gurrieri, S., Lauceri, R., Raudino, A., Scolaro, L. M., and Santoro, A. M. (1998) pH Modulation of Porphyrin Self-Assembly onto Polylysine. *J. Phys. Chem. B 102*, 8852−8857.

(21) Jankowska, K. I., Pagba, C. V., Piatnitski Chekler, E. L., Deshayes, K., and Piotrowiak, P. (2010) Electrostatic Docking of a Supramolecular Host-Guest Assembly to Cytochrome c Probed by Bidirectional Photoinduced Electron Transfer. *J. Am. Chem. Soc. 132*, 16423−16431.

(22) Martos, V., Bell, S. C., Santos, E., Isacoff, E. Y., Trauner, D., and de Mendoza, J. (2009) Calix[4]arene-based Conical-shaped Ligands for Voltage-dependent Potassium Channels. *Proc. Natl. Acad. Sci. U.S.A. 106*, 10482−10486.

(23) McGovern, R. E., Fernandes, H., Khan, A. R., Power, N. P., and Crowley, P. B. (2012) Protein Camouflage in Cytochrome c-calixarene Complexes. *Nat. Chem. 4*, 527−533.

(24) Chinai, J. M., Taylor, A. B., Ryno, L. M., Hargreaves, N. D., Morris, C. A., Hart, J. P., and Urbach, A. R. (2011) Molecular Recognition of Insulin by a Synthetic Receptor. *J. Am. Chem. Soc. 133*, 8810−8813.

(25) Dang, D. T., Schill, J., and Brunsveld, L. (2012) Cucurbit[8]uril-mediated Protein Homotetramerization. *Chem. Sci. 3*, 2679−2684.

(26) Aachmann, F. L., Otzen, D. E., Larsen, K. L., and Wimmer, R. (2003) Structural Background of Cyclodextrin-protein Interactions. *Protein Eng. 16*, 905−912.

(27) Kano, K., Watanabe, K., and Ishida, Y. (2008) Porphyrin J-aggregates Stabilized by Ferric Myoglobin in Neutral Aqueous Solution. *J. Phys. Chem. B 112*, 14402−14408.

(28) Forster, F., Webb, B., Krukenberg, K. A., Tsuruta, H., Agard, D. A., and Sali, A. (2008) Integration of Small-angle X-ray Scattering Data into Structural Modeling of Proteins and their Assemblies. *J. Mol. Biol. 382*, 1089−1106.

(29) Hammel, M. (2012) Validation of Macromolecular Flexibility in Solution by Small-angle X-ray Scattering (SAXS). *Eur. Biophys. J. 41*, 789−799.

(30) Madl, T., Gabel, F., and Sattler, M. (2011) NMR and Small-angle Scattering-based Structural Analysis of Protein Complexes in Solution. *J. Struct. Biol. 173*, 472−482.

(31) Putnam, C. D., Hammel, M., Hura, G. L., and Tainer, J. A. (2007) X-ray Solution Scattering (SAXS) Combined with Crystallography and Computation: Defining Accurate Macromolecular Structures, Conformations and Assemblies in Solution. *Q. Rev. Biophys. 40*, 191−285.

(32) Tiede, D. M., Mardis, K., and Zuo, X. (2009) X-ray Scattering Combined with Coordinate-based Analyses for Applications in Natural and Artificial Photosynthesis. *Photosynth. Res. 102*, 267−279.

(33) Guinier, A., and Fournet, G. (1955) *Small Angle Scattering of X-rays*, Wiley, New York.

(34) Lipfert, J., and Doniach, S. (2007) Small-angle X-ray Scattering from RNA, Proteins, and Protein Complexes. *Annu. Rev. Biophys. Biomol. Struct. 36*, 307−327.

(35) Svensson, B., Tiede, D. M., and Barry, B. A. (2002) Small-angle X-ray Scattering Studies of the Manganese-stabilizing Subunit in Photosystem II. *J. Phys. Chem. B 106*, 8485−8488.

(36) Svensson, B., Tiede, D. M., Nelson, D. R., and Barry, B. A. (2004) Structural Studies of the Manganese-stabilizing Subunit in Photosystem II. *Biophys. J. 86*, 1807−1812.

(37) Londer, Y. Y., Pokkuluri, P. R., Tiede, D. M., and Schiffer, M. (2002) Production and Preliminary Characterization of a Recombinant Triheme Cytochrome c7 from *Geobacter sulfurreducens* in *Escherichia coli*. *Biochim. Biophys. Acta 1554*, 202−211.

(38) Rambo, R. P., and Tainer, J. A. (2013) Super-Resolution in Solution X-ray Scattering and Its Applications to Structural Systems Biology. *Annu. Rev. Biophys. 42*, 415−441.
(39) Tiede, D. M., Zhang, R., and Seifert, S. (2002) Protein conformations explored by difference high-angle solution X-ray scattering: Oxidation state and temperature dependent changes in cytochrome c. *Biochemistry 41*, 6605−6614.
(40) Pokkuluri, P. R., Londer, Y. Y., Duke, N. E., Erickson, J., Pessanha, M., Salgueiro, C. A., and Schiffer, M. (2004) Structure of a novel c7-type three-heme cytochrome domain from a multidomain cytochrome c polymer. *Protein Sci. 13*, 1684−1692.
(41) Humphrey, W., Dalke, A., and Schulten, K. (1996) VMD: Visual Molecular Dynamics. *J. Mol. Graphics 14*, 33−38.
(42) MacKerell, A. D., Bashford, D., Bellot, M., Dunbrack, R. L., Jr., Evansec, J. D., Field, M. J., Fisher, S., Gao, J., Guo, H., Ha, S., Joseph, D., Kuchnir, L., Kuczera, K., Lau, F. T. K., Mattos, C., Michnick, S., Ngo, T., Nguyen, D. T., Prodhom, B., Reiher, I. W. E., Roux, B., Schlenkrich, M., Smith, J., Stote, R., Straub, J., Watanabe, M., Wiorkiewicz-Kuczera, J., Yin, D., and Karplus, M. (1998) All-atom Empirical Potential for Molecular Modeling and Dynamics Studies of Proteins. *J. Phys. Chem. B 102*, 3586−3616.
(43) Autenrieth, F., Tajkhorshid, E., Baudry, J., and Luthey-Schulten, Z. (2004) Classical Force Field Parameters for the Heme Prosthetic Group of Cytochrome c. *J. Comput. Chem. 25*, 1613−1622.
(44) Phillips, J. C., Braun, R., Wang, W., Gumbart, J. C., Tajkhorshid, E., Villa, E., Chipot, C., Skeel, R. D., Kale, L., and Schulten, K. (2005) Scalable Molecular Dynamics with NAMD. *J. Comput. Chem. 26*, 1781−1802.
(45) Zuo, X., and Tiede, D. M. (2005) Resolving Conflicting Crystallographic and NMR Models for Solution-State DNA with Solution X-ray Diffraction. *J. Am. Chem. Soc. 127*, 16−17.
(46) Devanathan, S., Salamon, Z., Tollin, G., Fitch, J. C., Meyer, T. E., Berry, E. A., and Cusanovich, M. A. (2007) Plasmon Waveguide Resonance Spectroscopic Evidence for Differential Binding of Oxidized and Reduced *Rhodobacter capsulatus* Cytochrome c_2 to the Cytochrome bc_1 Complex Mediated by the Conformation of the Rieske Iron-sulfur Protein. *Biochemistry 46*, 7138−7145.
(47) Rosen, D., Okamura, M. Y., and Feher, G. (1980) Interaction of Cytochrome c with Reaction Centers of *Rhodopseudomonas sphaerodies* R-26: Determination of Number of Binding Sites and Dissociation Constants by Equilibrium Dialysis. *Biochemistry 19*, 5687−5692.
(48) Mauk, M. R., Ferrer, J. C., and Mauk, A. G. (1994) Proton Linkage in Formation of the Cytochrome c-cytochrome c Peroxidase Complex: Electrostatic Properties of the High- and Low-affinity Cytochrome Binding Sites on the Peroxidase. *Biochemistry 33*, 12609−12614.
(49) Autenrieth, F., Tajkhorshid, E., Schulten, K., and Luthey-Schulten, Z. (2004) Role of Water in Transient Cytochrome c_2 docking. *J. Phys. Chem. B 108*, 20376−20387.
(50) Solmaz, S. R., and Hunte, C. (2008) Structure of Complex III with Bound Cytochrome c in Reduced State and Definition of a Minimal Core Interface for Electron Transfer. *J. Biol. Chem. 283*, 17542−17549.
(51) Ahmed, A. J., Smith, H. T., Smith, M. B., and Millett, F. S. (1978) Effect of Specific Lysine Modification on the Reduction of Cytochrome c by Succinate-cytochrome c Reductase. *Biochemistry 17*, 2479−2483.
(52) Rieder, R., and Bosshard, H. R. (1980) Comparison of the Binding Sites on Cytochrome c for Cytochrome c Oxidase, Cytochrome bc_1, and Cytochrome c_1. Differential Acetylation of Lysyl Residues in Free and Compelxed Cytochrome c. *J. Biol. Chem. 255*, 4732−4739.
(53) Smith, H. T., Ahmed, A. J., and Millett, F. (1981) Electrostatic Interaction of Cytochrome c with Cytochrome c_1 and Cytochrome c Oxidase. *J. Biol. Chem. 256*, 4984−4990.
(54) Speck, S. H., Ferguson-Miller, S., Osheroff, N., and Margoliash, E. (1979) Definition of Cytochrome c Binding Domains by Chemical Modification: Kinetics of Reaction with Beef Mitochondrial Reductase and Functional Organization of the Respiratory Chain. *Proc. Natl. Acad. Sci. U.S.A. 76*, 155−159.
(55) Pelletier, H., and Kraut, J. (1992) Crystal Structure of a Complex between Electron Transfer Partners, Cytochrome c Peroxidase and Cytochrome c. *Science 258*, 1748−1755.
(56) Volkov, A. N., Worrall, A. J., Holtzmann, E., and Ubbink, M. (2006) Solution Structure and Dynamics of the Complex between Cytochrome c and Cytochrome c Peroxidase Determined by Paramagnetic NMR. *Proc. Natl. Acad. Sci. U.S.A. 103*, 18945−18950.
(57) Hunte, C., Solmaz, S., and Lange, C. (2002) Electron Transfer between Yeast Cytochrome bc_1 Complex and Cytochrome c: A Structural Analysis. *Biochim. Biophys. Acta 1555*, 21−28.
(58) Lange, C., and Hunte, C. (2002) Crystal Structure of the Yeast Cytochrome bc_1 Complex with its Bound Substrate Cytochrome c. *Proc. Natl. Acad. Sci. U.S.A. 99*, 2800−2805.
(59) Adir, N., Axelrod, H. L., Beroza, P., Isaacson, R. A., Rogney, S. H., Okamura, M. Y., and Feher, G. (1996) Co-crystallization and Characterization of the Photosynthetic Reaction Center-cytochrome c_2 Complex from *Rhodobacter sphaeroides*. *Biochemistry 35*, 2535−2547.
(60) Axelrod, H. L., Abresch, E. C., Okamura, M. Y., Yeh, A. P., Rees, D. C., and Feher, G. (2002) X-ray Structure Determination of the Cytochrome c2:reaction Center Electron Transfer Complex from *Rhodobacter sphaeroides*. *J. Mol. Biol. 319*, 501−515.
(61) Pogorelov, T. V., Autenrieth, F., Roberts, E., and Luthey-Schulten, Z. A. (2007) Cytochrome c_2) Exit Strategy: Dissociation Studies and Evolutionary Implications. *J. Phys. Chem. B 111*, 618−634.
(62) Kokhan, O., Wraight, C. A., and Tajkhorshid, E. (2010) The Binding Interface of Cytochrome c and Cytochrome c_1 in the bc_1 Complex: Rationalizing the Role of Key Residues. *Biophys. J. 99*, 2647−2656.
(63) Dantas, J. M., Morgado, L., Catarino, T., Kokhan, O., Pokkuluri, P. R., and Salgueiro, C. A. (2014) Evidence for Interaction between the Triheme Cytochrome PpcA from *Geobacter sulfurreducens* and Anthrahydroquinone-2,6-sulfonate, an Analog of the Redox Active Components of Humic Substances. *Biochim. Biophys. Acta 1837*, 750−760.
(64) Rosell, F. I., Ferrer, J. C., and Mauk, A. G. (1998) Proton Linked Protein Conformational Switching: Definition of the Alkaline Conformational Transition of Yeast iso-1-Ferricytochrome c. *J. Am. Chem. Soc. 120*, 11234−11245.
(65) Dumortier, C., Meyer, T. E., and Cusanovich, M. A. (1999) Protein Dynamics: Imidazole Binding to Class I c-type Cytochromes. *Arch. Biochem. Biophys. 371*, 142−148.